Journal of Thermal Science Vol.31, No.5 (2022) 1642−1662

https://doi.org/10.1007/s11630-022-1656-z **Article ID: 1003-2169(2022)05-1642-21**

Mechanistic Insights into Effects of Outer Stage Flare Angle on Ignition and Flame Propagation of Separated Dual-Swirl Spray Flames

YANG Siheng[1], HUI Xin[1], ZHANG Chi[1*], QIAN Weijia[1], GAN Xiaohua[2]

1. National Key Laboratory of Science and Technology on Aero-Engine Aero-Thermodynamics, School of Energy and Power Engineering, Beihang University, Beijing 102206, China
2. Department of Mechanics and Aerospace Engineering, Southern University of Science and Technology, Shenzhen 518000, China

Abstract: The present work investigates the effects of outer stage flare angle on ignition and kernel propagation in a centrally staged optical model combustor based on the kernel dynamics analysis and laser diagnostics of flow and spray fields. Three outer stage flare angles of 8°, 16°, and 25° are researched, respectively. The better ignition performances are found for larger outer stage flare angles. Key properties such as the kernel velocity, kernel trajectory extracted from 6 kHz high-speed flame images are analyzed in combination with the flow and spray measured via Particle Image Velocimetry (PIV) and Planar Mie Scattering (PMie). Results show that the larger outer stage flare angle imposes a larger opening angle of outer swirl jet (SWJ), shifting the vortex in outer recirculation zone (ORZ) and inner recirculation zone (IRZ) upstream. The spray distribution of a smaller flare angle exhibits a fuel-lean zone near the igniter and this is attributed to the presence of low-angle outer swirl jet that prevents the fuel droplets from arriving at the igniter vicinity. The flame kernel propagates along the path where the strain rate and velocity decrease and the spray droplet density is within the flammable limits. A lower outer stage flare angle increases the strain rate and velocity at the early phase of flame propagation, leading to a longer propagation route and thus increasing the risk of ignition failure.

Keywords: spray ignition, flame propagation, spray distribution, separated dual-swirl

1. Introduction

Advanced civil aero-engines have adopted lean-burn technology to meet pollutant regulations mandated by the International Civil Aviation Organization (ICAO). Generally, the lean combustion techniques that limit NO_x formations are reported to suffer from severe ignition issues due to significant flow convection effects and the starvation of fuel [1, 2]. It is urgent for civil aviation engine designers to explore effective strategies for shifting the ignition boundary to leaner conditions. A better understanding of the forced ignition in such flames is thus necessary for optimizing the ignition performance in lean-burn combustors.

Successful ignition in a realistic gas turbine combustor requires several different phases. The forced ignition process in a single-sector combustor is usually summarized in the literature to contain 3 phases: kernel generation, flame growth, and the flame establishment [2–4]. However, the third phase (flame establishment) is

Received: Nov 15, 2021 AE: ZHAO Dan Corresponding author: ZHANG Chi E-mail: zhangchi@buaa.edu.cn

Nomenclature

c	gray intensity
d	distance to the origin/m
FAR	fuel to air ratio
L	kernel propagation distance/m
P^*	total pressure/Pa
R	radial coordinate
R_v	swirl radial velocity ratio
S	strain rate/s^{-1}
SMD	sauter mean diameter/m
T^*	total temperature/K
t	time/s
V	air velocity/$m \cdot s^{-1}$
Y	axial coordinate

Greek symbols

α	half spray cone angle/(°)
θ	outer stage flare angle/(°)
σ	total pressure drop across the combustor
ω	vorticity/s^{-1}

Subscripts

1	combustor inlet
2	combustor outlet
ref	reference value
YR	tensor in the Y-R plane

Abbreviations

ICAO	international civil aviation organization
IRZ	inner recirculation zone
ISL	inner shear layer
LDI	lean direct injection
LLO	lean light off
LPP	lean premixed prevaporized
LRZ	lip recirculation zone
ORZ	outer recirculation zone
OSL	outer shear layer
PIV	particle image velocimetry
PMie	planar mie scattering
RR	rolls royce
SWJ	swirl jets
TAPS	twin annular premixing swirler
TeLESS	technology of low emission of stirred swirl

defined broadly and needs more detailed description. Previous studies have reported a special "growth delay" period before successful ignition in some realistic combustors [5–7], during which the flame luminosity is low. This phenomenon has also been observed in laboratory-scale burners [8] and has been defined as "ignition delay" [9], which can be an intrinsic phase during a successful ignition event. These findings prove that the forced ignition process includes additional phases that have not been investigated previously and need to be examined closely, especially on the flame morphology during each phase in the ignition process.

Flow aerodynamics is one of the key factors controlling the ignition and flame propagation of turbulent spray flames [4]. Despite the significant importance of practical application, the studies examining the correlation between forced ignition and flow patterns in realistic combustors are relatively limited. High-altitude relight inside a lean-direct-injection (LDI) combustor [6] shows that the flame motion during the ignition process is dominated by cold flow convection and the high flow velocity leads to a rapid disintegration of kernel. The effects of swirling intensity on the ignition performance have been investigated in a swirl cup combustor [10] and fuel staged lean premixed prevaporized (LPP) combustors [5, 11]. Their results indicate that the higher swirling intensity is beneficial for inducing a recirculation structure and enhancing the turbulence intensity, thus facilitating the ignition performance. Fu et al. [12] performed measurements on the ignition performance in a LPP combustor and analyzed the correlation between ignition process and flow field using numerical simulations. The recirculation zone in the combustor propagates the ignition kernel upstream and favors the establishment of flame. Swirling flows are usually introduced in gas turbine combustors and contains complex fluid mechanic behaviors that exhibit several typical flow regions [13]: the annular swirling jet, the inner shear layer (ISL), the outer shear layer (OSL), the outer recirculation zone (ORZ), and the inner recirculation zone (IRZ). Recent trend of lean-burn combustors features a large amount of air injected from swirl injectors [14], generating stronger swirling jets. While previous studies provide a valuable basis for understanding the flow effects on forced ignition, there is still a lack of data focusing on the swirl jet aerodynamics in realistic lean-burn combustors and its effect on the forced ignition characteristics. In the present study, we aim to obtain a better understanding of this issue by proposing a geometric parameter, i.e., flare angle, affecting the swirl jet patterns and to reveal the underlying mechanisms of different ignition performances under various flare angles.

For spray flame ignition in realistic combustors, the fuel droplets are not uniformly dispersed and hence the non-uniform spatial distribution of spray droplets must be considered. Recent work in some laboratory-scale

spray flames [15–17] have demonstrated that ignition inside a spray with a large amount of flammable fuel-air mixtures is more likely to result in a successful flame establishment. In more practical researches, few data [11, 18] are available focusing on the correlation between non-uniform spray distribution and ignition characteristics. In fact, the dispersions of spray droplets are largely impacted by the surrounding flow velocities. However, no detailed guidance exists on which type of spray distribution facilitates spray ignition in realistic complex flow patterns and on the effects of swirl aerodynamics on the fuel droplets transportation within combustors. Another objective of this work is to obtain a better understanding of how the change of swirl jet pattern can impact the spray distribution and further influence the ignition characteristics.

As mentioned before, the ignition in lean-burn combustors is an increasingly important issue. Among the lean-burn technologies of gas turbine combustors, staged LPP combustion proves to have the advantage of low pollutant emissions and good flame stability and is employed in a range of configurations, such as twin annular premixing swirler (TAPS) [19], Lean-Burn of Rolls-Royce (R-R) [20], and technology of low emission of stirred swirl (TeLESS-I) [12]. These designs adopt the centrally staged annular configuration that is comprised of two stages: the inner pilot stage and the outer main stage. The pilot stage in the center uses non-premixed combustion to stabilize the flame, and the main stage in the outer annular uses LPP combustion to control NO_x emissions operating at high power modes. In the present study, we examine the ignition characteristics in a centrally staged model combustor that is more relevant to practical gas turbine combustors.

Based on the above discussions, the present study aims to investigate the effects of outer stage flare angle on the ignition and flame propagation in a centrally staged model combustor and to correlate the resulting ignition characteristics with the flow properties and spray distribution, in order to provide guidance for optimizing ignition performance in swirl-stabilized combustors. The rest of the paper is organized as follows. First, the experimental setup and methods section shows the combustor configuration, the ignition test system, and diagnostic methods. This is followed by ignition performances of different outer stage flare angles. In order to identify the correlation between flare angle and outer swirl radial velocity ratio and to illustrate why the flare angle has a significant impact on the ignition performance, the spray pattern and non-reacting flow field have been examined using optical diagnostic methods. Then the whole ignition process is divided into several individual phases and effects of flare angle on the ignition phases are analyzed focusing on the kernel motions and the flame morphology. Finally, the effects of flare angle on the flame propagation are discussed and guidance for improving ignition performances in swirl-stabilized combustors is provided.

2. Experimental Setup and Methods

2.1 Model combustor

Experiments are carried out in an optical version of the TeLESS-II combustor developed by Beihang University [5, 21]. Its schematic is shown in Fig. 1. The combustor adopts a centrally staged configuration and the swirl injector contains two stages: the inner pilot stage and the outer main stage. The inner pilot stage is a typical swirl cup structure consisting of three main components: a simplex nozzle, a venturi tube, and dual radial swirlers; the outer main stage consists of an axial swirler and premixing channels. The detailed design parameters of the combustor are listed in Table 1. The model combustor has transparent quartz windows on the

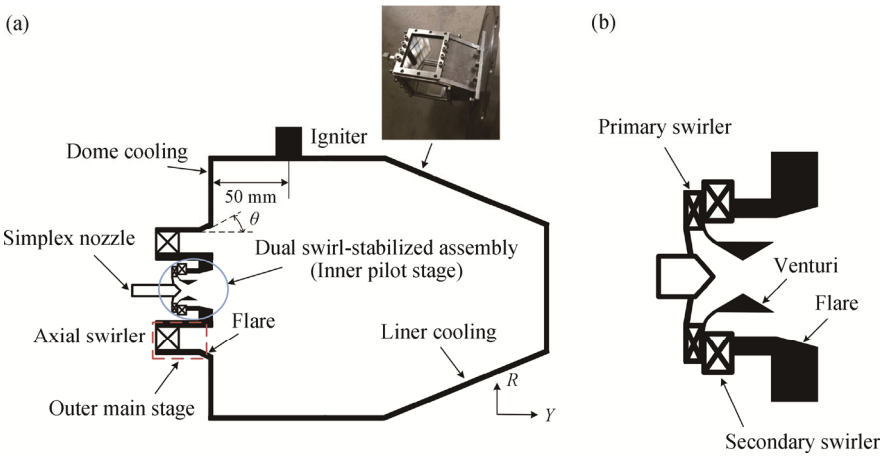

Fig. 1 (a) Schematic of the model combustor and definition of the flare angle. The inner pilot stage and the outer main stage are marked for easy distinguishment. (b) Sketch of dual-radial swirl-stabilized assembly (Inner pilot stage), reproduced from Ref. [23], with permission from Elsevier

Table 1 Parameters of the model combustor

Outer main stage	Axial swirler	Swirl number	0.5
		Vane angle	30°
Inner pilot stage	Simplex nozzle	Flow number	20.8 kg/(h·MPa$^{0.5}$)
		Nozzle type	90° hollow cone
	Primary radial swirler	Swirl number	0.6
	Secondary radial swirler	Swirl number	0.8

side walls to provide optical access for measurements. A surface-discharge igniter is used with the location fixed at 50 mm downstream of the injector exit. The igniter is installed on the upper wall of the combustor via a threaded hole, and the igniter tip is flush with the wall. The flare angle θ is a variable in the present study. It is defined as the angle between the main stage flare and the axial direction (Fig. 1). Three flare angles of the outer main stage, i.e., 8°, 16°, and 25°, are investigated in the present study. The modification of outer stage flare angle influences the outer swirl radial velocity ratio R_v. It is defined as V_r/V, where V_r is the radial velocity and V is the velocity magnitude in swirl jet zones. The radial velocity ratios for three flare angles are measured using Particle Image Velocimetry (PIV), and results are analyzed in Section 3.2 (Fig. 6).

2.2 Ignition test system

Ignition test system is comprised of an air supply system, a fuel system, an ignition system, and a data acquisition system, as shown in Fig. 2. Compressed air from a compressor is controlled by an electric valve and the air mass flow rate is measured by an orifice plate (±1%). The mass flow rate of liquid fuel (Chinese aviation kerosene RP-3 whose compositions are presented in our previous study [22]) is measured by a Coriolis mass flowmeter. In addition, two pressure probes and a thermocouple are used to measure the inlet total pressure P_1^*, outlet total pressure P_2^*, and inlet total temperature T_1^* of the combustor with the precision of 0.5%. The igniter is connected to a high-energy power supply system (XDH-12 from KRE) and the stored energy is 12 J. This unit gives multiple sparks with an output energy of 1.93 J/spark and a frequency of 10 Hz. Details about the ignition system can be found in Ref. [23].

Only the pilot nozzle is turned on during the ignition experiments. The ignition experiments are carried out at ambient temperature and pressure. Ignition boundaries are tested at total pressure drop (σ) ranging from 1% to 5%. The total pressure drop across the combustor is defined as

$$\sigma = \frac{P_1^* - P_2^*}{P_1^*} \tag{1}$$

At a given combustor pressure drop, the procedure to obtain a lean ignition limit is to gradually reduce the fuel to air ratio (FAR) until an ignition failure happens. An ignition failure is defined as an event that stable flame cannot establish and stabilize within 10 seconds (suggested by Lefebvre [3]) after the igniter works. To ensure the repeatability of the test results, successful ignition events are conducted ten times for each pressure drop condition, and the minimum lean light off (LLO) FAR is averaged from ten experimental data. The uncertainty of the ignition boundary is estimated from the standard deviation related to its mean. In the present work, the maximum uncertainty of the ignition boundary (LLO FAR) is calculated as 0.0011.

2.3 Diagnostic methods

It is necessary to analyse the velocity fields, spray distribution, and flame kernel propagation to reveal the effects of outer stage flare angle on the flow aerodynamics, spray characteristics, flame propagation and thus on the ignition performance. For this purpose, several diagnostic methods including PIV, Planar Mie Scattering (PMie), and High-speed imaging have been employed in the present study. All the operating conditions studied are presented in Table 2.

2.3.1 Particle Image Velocimetry

PIV setup comprises a frequency-doubled double-cavity Nd:YAG laser running at 10 Hz, a double-shutter CCD camera (1376 pixels × 1024 pixels), and a programmable timing unit. The 532 nm laser beam is formed into a 1 mm thickness laser sheet using a cylindrical telescope. Mie scattering signals from the illumination of the tracer particles by the laser sheet are filtered by a narrowband optical filter (532 nm ± 5 nm) and captured by the CCD camera. The tracer particles are TiO_2 solid particles with the nominal diameter of 1 μm. The mass flow rate of the air carrying the particles is about 10% of the mainstream. Seeding particles are injected into the mainstream about 1.4 m upstream of the swirl injector exit plane to ensure the tracer particles are uniformly distributed. The instantaneous air velocity fields are post-processed from raw Mie scattering images via a commercial PIV software. The multi-pass cross-correlation is carried out via the commercial

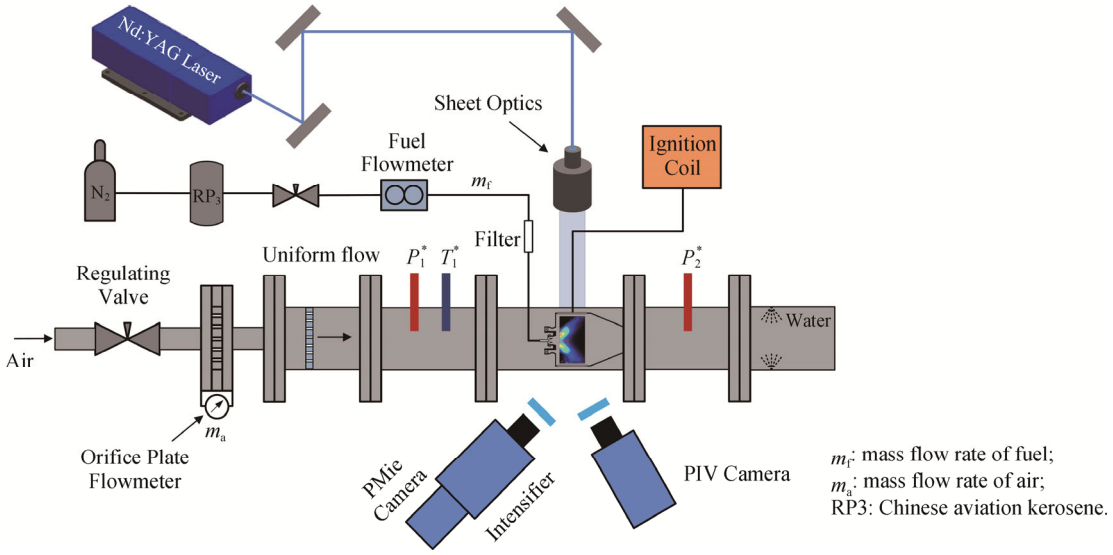

Fig. 2 Schematic of the ignition test system and laser diagnostic system, reproduced from Ref. [23], with permission from Elsevier

Table 2 Operating conditions

Case	θ/(°)	Methods	σ	FAR
Nonreacting	8, 16, 25	PIV	3%	0
	8, 16, 25	PMIE	2%–4%	0.02, 0.025, 0.03
Reacting	8, 16, 25	Ignition Performance	1%–5%	LLO FAR
	8, 25	High-Speed Imaging	3%	0.025

algorithm (LaVision Davis 8.4). A interrogation window size for vector processing is chosen as 16×16 pixles^2 and the overlap is 50%. The 2-D spatial resolution for the velocity vector is 1.58×1.58 mm^2. A peak ratio of 3 is selected for velocity calculating with the 2-D reconstruction error of 0.5 pixel. A series of 1000 continuous raw particle images are selected to calculate 500 instantaneous velocity fields. The 500 instantaneous velocity fields are averaged by the software Matlab to obtain the mean velocity fields. Detailed information about the PIV setup can be found in Ref. [11].

2.3.2 Planar Mie Scattering

The PMie system consists of a pulsed Nd:YAG laser running at 30 Hz and providing a 532 nm laser beam. The scattering signal produced from the illumination of fuel droplets is detected and collected by a CCD camera and an image intensifier. A narrow bandpass optical filter centered at 532 nm with a 5 nm spectral width is used to collect the Mie scattering signals. The effective pixel detecting the Mie scattering signal is 295 pixels × 548 pixels and the effective area is 70 mm×130 mm, leading to a magnification factor of 0.237 mm/pixel. The time-averaged spray distribution is obtained from the processing of 500 transient images and then subtracting the background signal. To compare the time-averaged spray distribution from different conditions, the intensities of Mie scattering signals are normalized to the maximum value for each operating condition.

2.3.3 High-speed imaging

High-speed imaging is used to record the flame propagation during the whole ignition process. The flame spontaneous radiation is captured by a high-speed camera (X-Stream Vision XS-3, 1024×1024 pixels^2) with a frame rate of 6 kHz and exposure time of 25 μs, which is able to capture the kernel behavior during the whole ignition process. The effective imaging size is 553×657 pixels^2 and the size of the effective region is 110 mm×130 mm, leading to a magnification ratio of 0.2 mm/pixel.

2.4 Image data processing

Gradient-based quantities such as the strain rate and vorticity are calculated by the 2D flow velocity components from PIV tests to provide useful information for analyzing the correlation between spark ignition and flow properties. For a planar 2D velocity field, the out-of-plane vorticity (ω_X) and the strain tensor in the Y-R plane (S_{YR}) are calculated from the following expressions:

$$\omega_X = \frac{\partial V_Y}{\partial R} - \frac{\partial V_R}{\partial Y} \tag{2}$$

$$S_{YR} = \frac{1}{2}\left(\frac{\partial V_Y}{\partial R} + \frac{\partial V_R}{\partial Y}\right) \tag{3}$$

where the quantity V_i represents the velocity components in the direction i.

Flame kernel area, kernel trajectories, kernel velocities and kernel propagation regions during the ignition process are important parameters for illustrating the kernel motion behaviors. The procedure of image processing is shown in Fig. 3. The 2D gray scale flame emission images are first binarized using the threshold segmentation method with the threshold being determined by Otsu's method [24] to obtain the projected flame region. As shown in Fig. 3(b), the binarized images are white in flame region (assigned ones c=1) and black in unburned region (assigned zeros c=0). The c represents the gray intensities of the binarized images. The projected flame area is computed by counting the total pixels involved in the flame projected region. The flame kernel centroid position (y_k, r_k) is calculated from each frame by averaging the coordinate positions of points in flame region using Eqs. (4) and (5). The kernel trajectories and velocities are then obtained from a sequence of kernel centroid positions. All binary images are integrated to obtain the flame propagation regions.

$$y_k = \frac{1}{n}\left(\sum_{i=1}^{n} y_i\,(c=1)\right) \tag{4}$$

$$r_k = \frac{1}{n}\left(\sum_{i=1}^{n} r_i\,(c=1)\right) \tag{5}$$

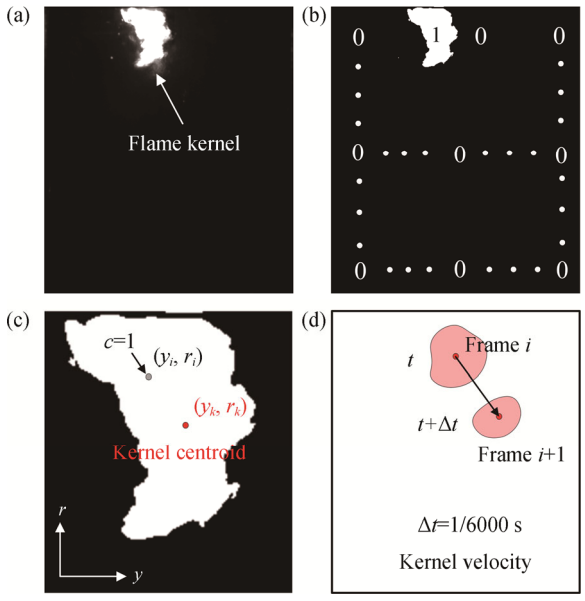

Fig. 3 (a) Gray scale flame image; (b) binarized result of (a) with Otsu's method; (c) calculation of kernel centroid; (d) calculation of kernel velocity

3. Results and Discussion

3.1 Ignition performances

Lean light off (LLO) boundary can be obtained based on the minimum LLO FARs for successful ignition at different pressure drops σ, as described in Section 2.2. Ignition performance test data of three main stage flare angles and the comparison of the ignition boundaries are shown in Fig. 4. The ignition performance is the worst at σ = 1% for all three flare angles. Minimum LLO FARs gradually decrease when the pressure drops increase from 1% to 5% for the cases of θ=16° and 25°. In contrast, an increase of minimum LLO FARs is observed for θ=8° as σ further increases from 4% to 5%. The effects of pressure drop on the overall ignition performance are analyzed as follows. The main factors influencing the spray ignition are the ignition system, flow variables, and fuel parameters [3]. Effect of ignition system is ignorable since experiments are carried out using the same ignition unit [23] that gives stable sparks. With the increase of pressure drop, there are two competitive effects on ignition performance: fuel parameters and flow properties. The combustor reference velocity V_{ref} increases from 6.2 m/s to 17.7 m/s as σ increases from 1% to 5%. The increase in flow velocity and turbulence increases the loss of heat in a linear way [25] during the initial phase of kernel generation and subsequent period of flame propagation, impairing the ignition performance.

In practical combustors, obtaining small fuel droplets sizes is key for improving ignition performance. The Sauter Mean Diameter (SMD) of fuel droplets has been measured via a particle sizer (MALVERN LSA-II) to evaluate the effects of operating conditions on the spray droplet size, shown in Table 3. The SMD for three flare angles is approximately the same, confirming the negligible effect of flare angle on the fuel atomization. As expected, it is found that the fuel atomization significantly improves with the increase of pressure drop due to the higher aerodynamic forces. As σ increases, the effects of spray characteristics exceed the effects of flow velocity and turbulence at most conditions, and a better ignition performance is obtained. Under the pressure drop of 4%, the two effects come to a balance when the flare angle is 8°, and the ignition performance is optimized. Specific to the case of θ=8°, a convection effect from the high speed swirl jet poses a significant threat to the existence and propagation of flame kernels at σ =5%, leading to an increase in LLO FAR. The mechanism of flow on kernel propagation is further illustrated in Section 3.4.2.

Comparing ignition boundaries of the three cases, it is found that lean ignition limit of the flare angle of 25° is lower than that of the flare angle of 8° and 16°. This demonstrates that the increase of the flare angle can facilitate the ignition performance of centrally staged LPP combustors. The differences in the ignition performance between the three flare angles should be

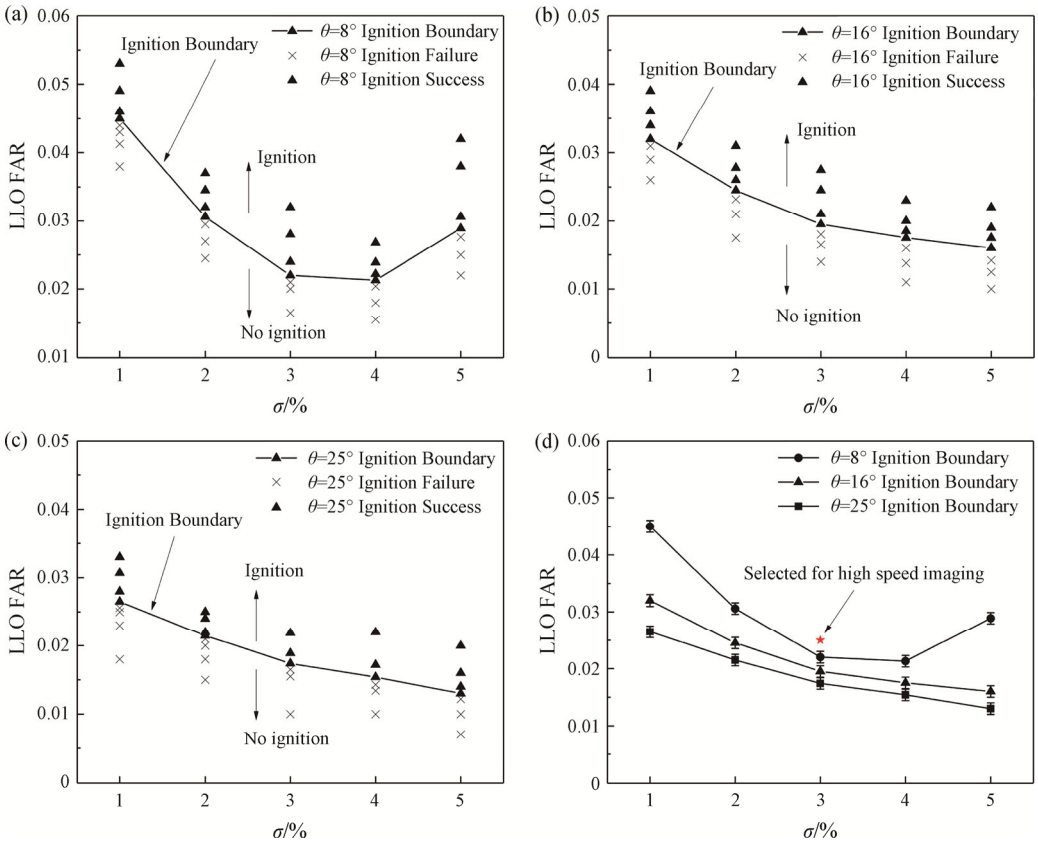

Fig. 4 Test data of ignition performance for three main stage flare angles (a) θ=8°, (b) θ=16°, (c) θ=25°, and (d) comparison of three cases. Error bars indicate the inaccuracy in determining the ignition boundary, caused by the errors/uncertainty in minimum LLO FAR (calculated from mass flow rates of fuel and air) from repeatability tests.

Table 3 Fuel droplets SMD and air reference velocity V_{ref} at varying σ. SMD_1, SMD_2, and SMD_3 are measured at FAR= 0.012, 0.019, and 0.031 respectively

σ/%	V_{ref}/m·s^{-1}	SMD_1/μm	SMD_2/μm	SMD_3/μm
1	6.2	74.3	90.9	96.5
2	9.8	49.7	56.5	58.0
3	13.1	39.8	42.2	45.9
4	15.9	31.4	35.2	38.8
5	17.7	26.5	32.0	34.4

analyzed from the perspective of local aerodynamics, spray dispersion, and their correlation with the ignition process. Previous studies show that regions of high velocity, strain rate, and fuel starvation are not favorable for kernel generation and upstream flame propagation [2, 15]. In a swirl-stabilized combustor, the exit of swirler is always characterized by high-speed jets. The increase of flare angle may induce a larger angle of high-speed jet flow that creates regions of low velocity and appropriate spray concentration. These factors may lead to a better ignition performance for a larger flare angle. In order to confirm the mechanism of the flare angle on ignition performance, PIV and PMie tests are carried out to obtain the flow field and spray distribution. In addition, a high-speed camera is used to record ignition transient processes at the operating condition as marked in Fig. 4(d).

3.2 Flow field

Fig. 5 presents the averaged air velocity fields (left) and typical instantaneous velocity fields (right) for θ=8°, 16°, and 25°. The color of the streamline plots represents the absolute velocity magnitude and the arrows indicate the velocity vectors. The resulting flow field features a complex structure that consists of two swirl jets (SWJ) entering the combustor from the inner and outer swirlers, an inner recirculation zone (IRZ), a lip recirculation zone (LRZ), and an outer recirculation zone (ORZ).

As shown, the inner and outer SWJ are represented by regions with high axial velocities. The LRZ is located approximately R=18 mm–28 mm after the lip structure. It is a unique flow feature in centrally staged LPP combustors and is formed by the flow separation, playing an important role in flame stabilization. Two SWJs from the inner and outer swirler are separated by LRZ and merge downstream, generating a complex separated dual-swirl flow pattern. The IRZ is one of the

fundamental features of swirl flows, which is formed by the axial pressure gradient associated with the occurrence of vortex breakdown. The vortex breakdown is usually manifested as a stagnation point followed by a region of reverse flow (IRZ) [26–28]. The upper stagnation point is found inside the swirl cup, which is beyond the PIV test domain (Y<2 mm). Two main vortices in IRZ are found downstream of the igniter, which plays an important role in early phases of kernel propagation during the ignition process (discussed in Sections 3.4 and 3.5). An ORZ is generated outside the outer SWJ due to the forced flow separation after the rapid expansion of the injector. High-velocity gradients occur between the SWJs and the surrounding flow, generating shear layers (ISL, OSL).

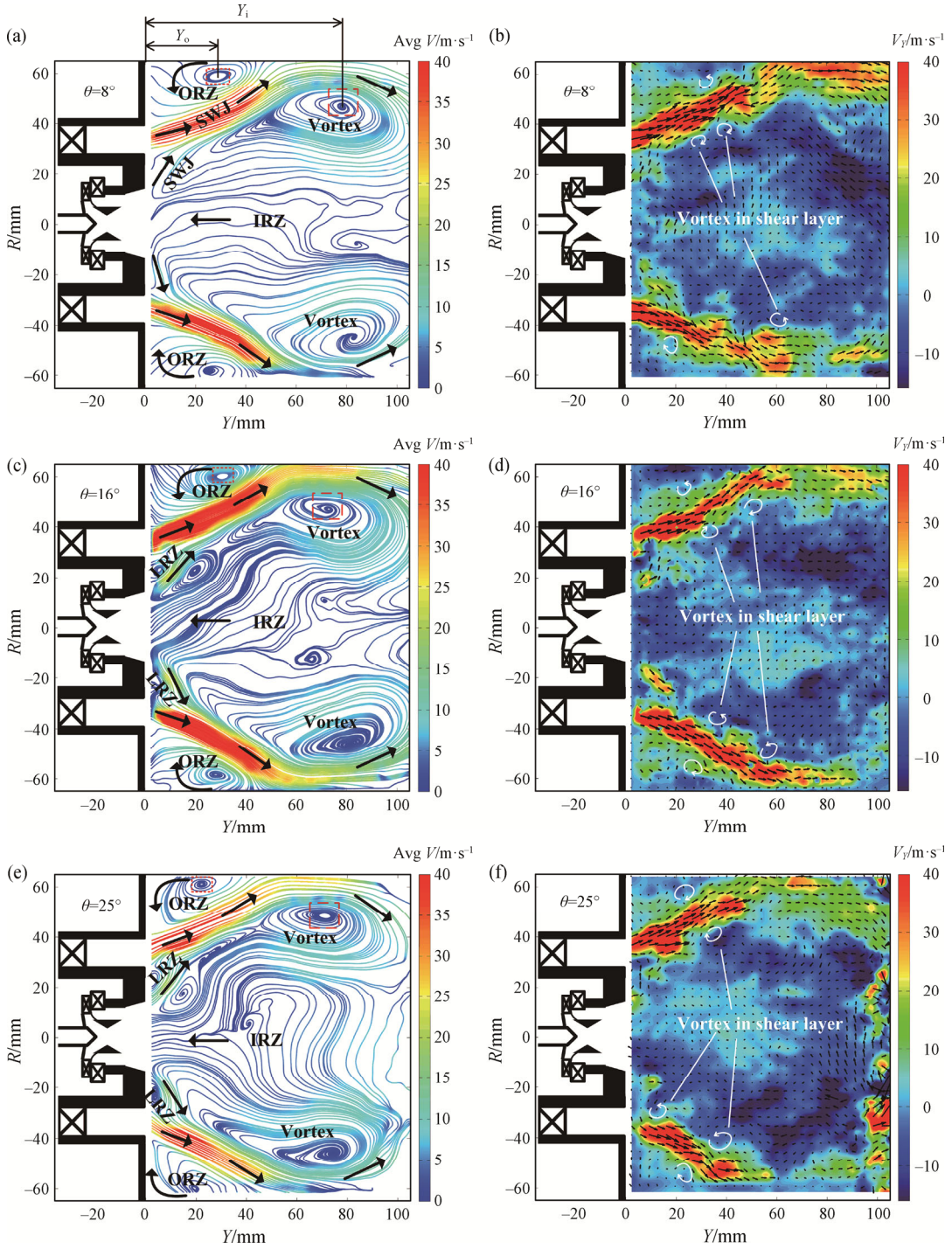

Fig. 5 Average velocity fields (left) and instantaneous velocity fields (right) for the main stage flare angle of 8°, 16°, and 25° at the total pressure drop of 3%. The colors in streamline plots represent the absolute velocity magnitudes and arrows indicate the velocity vectors.

Differences in the average flow between the three configurations are revealed in Fig. 5. In the case of θ=25°, the cone-shaped swirl jets injected from the main stage open quickly to touch the liner wall at Y≈60 mm with a larger cone angle, and a large IRZ is formed inside the inner shear layer (ISL) of main swirl jets. The comparing configuration of θ=8° presents cone-shaped swirl jets that penetrate further downstream at the injector outlet with a smaller opening angle. The IRZ between the main swirl jets is displaced downwards and shrinks due to the smaller opening angle of outer swirl jets. It is seen from the streamline plots that the axial positions of the outer vortex core (Y_o) and the inner vortex core (Y_i) are largely dependent on the swirl jets. The vortexes appear displaced downwards with the core of outer vortex and inner vortex shifted to Y_o≈28 mm and Y_i ≈78 mm for θ=8°, whereas for θ=25°, these two vortexes move upstream to Y_o≈22 mm and Y_i≈72 mm. The decrease of flare angle enhances the flow separation at the corner and shifts the outer vortex downstream. Moreover, a smaller opening angle of the outer SWJ induces the inner vortex downstream. It is further noted that there are no indications of a strong LRZ and vortex behind the lip for θ=8°. This indicates that the small flare angle weakens the separation between inner SWJ and outer SWJ, inhibiting the LRZ.

The swirl radial velocity ratio (R_v) is an important dimensionless quantity controlling the swirl jets pattern, defined as the ratio of radial velocity to the velocity magnitude (V_r/V). Since only the axial and radial velocity components are measured, the 2D velocity magnitude V is calculated by the square root of the two velocity components. In fact, the change of the flare angle has a direct impact on the radial velocity ratio of swirl jets from the outer stage. To illustrate the correlation between the swirl radial velocity ratio and the flare angle, the jet zones and radial velocity ratio of jet zones (where V_Y>30 m/s) for the θ=8°, 16°, and 25° are shown in Fig. 6. The jet zones are plotted by the iso-lines of axial velocity being 30 m/s and the dimensionless velocity R_v is extracted from the jet zones. It is seen that the swirl jet zones move inwardly when decreasing flare angle θ from 25° to 8°. These flow patterns are associated with the radial velocity ratio induced by the change of flare angle. At Y=3.5 mm, the dimensionless velocity R_v increases monotonously from 0.23 to 0.4 when the flare angle θ increases from 8° to 25°.

Some gradient-based quantities such as the vorticity and strain tensor can provide useful information that further illustrates the different ignition performances. The vorticity and strain rate are computed using the 2D flow velocity components from PIV measurements, as detailed in Section 2.4. Fig. 7 shows the contours of the calculated vorticity and strain rate in the Y-R plane for θ =25°. Positive and negative values of vorticity (red and blue) represent the counterclockwise and clockwise rotation of flow on the upper side of the flow field. High vorticity of more than 6000 s^{-1} occurs at the interfaces between the SWJ and surrounding recirculation flow, the ORZ and IRZ. The strain rate distribution appears similar to the vorticity field, implying the dominance of shear effect in the gradient term. The high strain rate of 2500 s^{-1} in the shear layers (OSL, ISL) means strong fluid deformation, indicating the high-velocity gradients from opposing directions of flow. The axial locations selected for the comparison of profiles of strain rates between different flare angles are shown in Fig. 7(a). It should be noted that the igniter is located at Y=50 mm, thus this location is selected for comparing the flow properties at the vicinity of spark.

Fig. 8 shows the comparison of mean strain rates between different flare angles at selected axial locations. The strain rates show different trends for the three configurations studied. Compared to θ=8°, the high strain

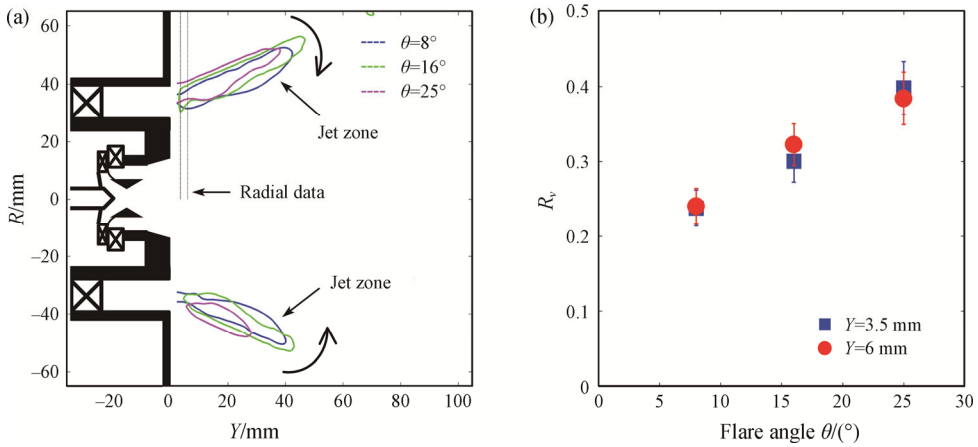

Fig. 6 Comparison of main stage jet zones (a) and radial velocity ratio R_v extracted from jet zones (b) for the main stage flare angle of 8°, 16°, and 25° at the total pressure drop of 3%

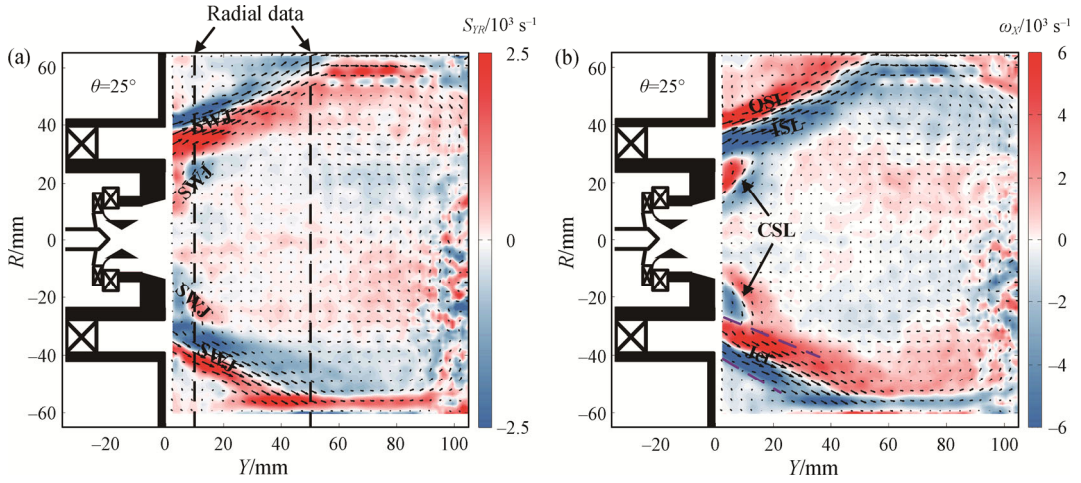

Fig. 7 Contours of (a) mean strain rate S_{YR} and (b) mean vorticity ω_X in the Y-R plane for θ=25°

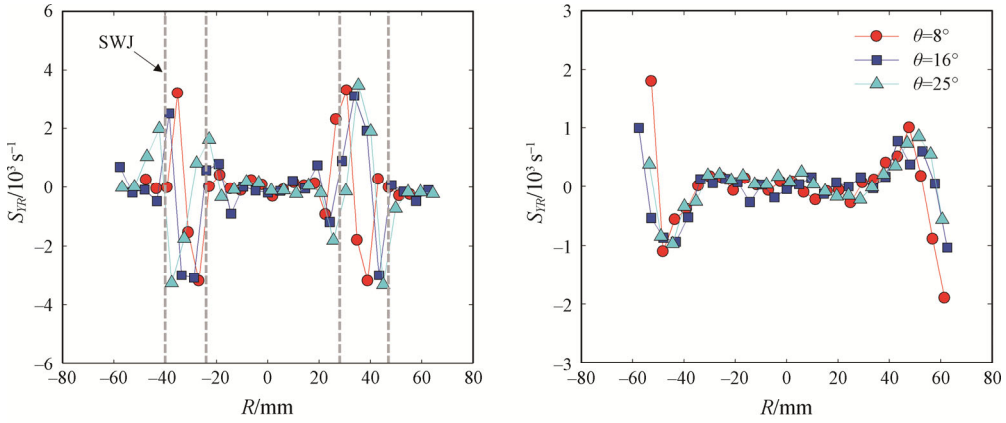

Fig. 8 Profiles of time-averaged strain rate S_{YR} in the Y-R plane for θ=8°, 16° and 25° at selected axial locations

rate from SWJ for θ=25° is found at a larger radial position, appearing that the swirl jets shift outward and lead to a larger opening angle. At the spark location (Y=50.3 mm), the strain rate is found high near the liner wall and decreases to zero at the center. A higher value of strain rate is seen near the spark location for smaller flare angles (θ=8°), which indicates a stronger stretching effect on the flame kernels during the kernel formation and initial propagation.

The effects of flare angle on the ignition performance are now concluded by analyzing the key flow features, flow transitions, and their relations with the forced ignition. As shown in Fig. 9, five main regions constitute the complex separated swirl flow in centrally stage LPP combustors. Forced ignition in a single sector needs 3 phases: kernel generation, flame growth, and flame establishment [2, 3]. Four ignition processes in such a complex flow are analyzed. The ignition process I denotes that the kernel propagates upstream and reaches the ORZ. The ignition process II is that the kernel

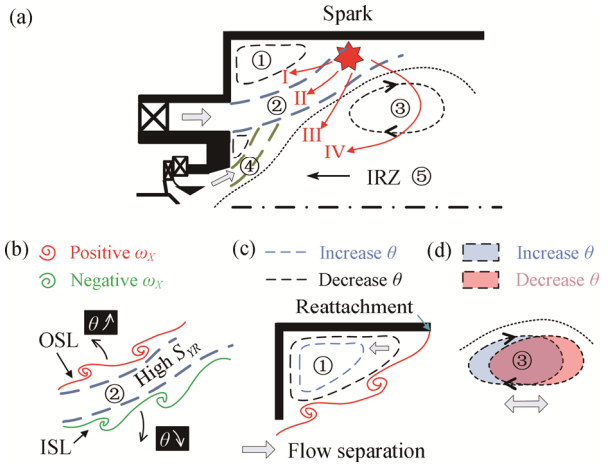

Fig. 9 (a) Key flow features in the present centrally staged LPP combustor and their relation with spark ignition. Transition of flow patterns for varying θ, focusing on three main regions: (b) SWJ, (c) ORZ, and (d) Toroidal vortex in IRZ

propagates upstream against the SWJ. The SWJ features high strain rate and vorticity combined with small vortices in shear layers. The high strain rate and velocity in SWJ pose a great threat for kernel generation and flame propagation. ORZ is also an unfavorable zone with low ignition probabilities [29]. The kernels are impossible to survive and establish flame successfully for processes I and II. In fact, the process IV is exactly the typical successful ignition process (discussed in Section 3.4). The vortex in IRZ associated to vortex breakdown (region ③) plays an important role in capturing the flame kernel and transporting it upstream.

Combining the findings from above, the effects of flare angle on the present separated dual-swirl are threefold: (1) the increase of θ suppresses the flow separation at the corner, shifting the separating shear layer and the ORZ (unfavorable region of ignition) upstream; (2) the larger flare angle increases the swirl radial velocity ratio that induces larger opening angle of SWJ. This decreases the strain rate at the spark location and facilitates the early phase of the ignition process; (3) the vortex in IRZ moves upstream with the increase of θ, which is beneficial for the upstream flame propagation. These flow transitions facilitate the process of kernel generation and subsequent flame propagation, thus improving the ignition performance. Above is the preliminary discussion, the effects of flare angle on the ignition process are detailed in Section 3.4.

3.3 Spray droplets distribution

For spray flame ignition, spray spatial distribution is one of the key factors controlling ignition processes. The Mie scattering intensity of the droplets is proportional to their total surface area and hence the Mie signal intensities can be used to show the spray droplets concentration qualitatively [30, 31]. Spray distributions for θ=8° and 25° at several pressure drops and FARs are presented in Fig. 10 and Fig. 11. To compare spray distribution between conditions at the same relative scale, the Mie scattering intensities are normalized to the maximum value for each condition. The white contour lines are plotted to visualize the spray cone pattern. In the figures, a slight asymmetry can be observed at the spray cores. This is due to the laser absorption by fuel droplets, especially in the spray core region. The time-averaged images reveal the typical spray pattern of the hollow cone structure in a separated dual-swirl flow field. High spray concentration (spray cone core) is found at the pilot swirler outlet, corresponding to inner swirl in the flow field. Almost no spray droplets are distributed at the exit of outer swirler channel due to the high air velocity in the outer SWJ. Low spray concentration is observed at the center of combustor that features the backflow.

The spray half cone angle a is defined and estimated in this study. The central points of spray cone (y_c, r_c) are first obtained by searching the points with the maximum distance (d_{max}) from the origin along the isoline. As shown in the top of Fig. 10, the distance d between points on an isoline and the origin (0, 0) is calculated as $(y_i^2+r_i^2)^{0.5}$. The core line is obtained by fitting the central points (y_c, r_c), where the subscript c indicates the central position. The half cone angle a is then defined as the angle between the core line and the axial direction. It is found that the pressure drop and FAR have significant influences on the spray half cone angle a. Increasing σ from 2% to 4%, the half cone angle a is observed to increase from 32° to 48° (for θ=8°). This is illustrated by the greater swirl-induced centrifugal forces on the fuel droplets that enhance the radial transportation and dispersion of spray droplets. The droplets obtain a higher initial tangential velocity at a higher fuel supply pressure, as expected, the spray cone angle increases with the FAR at constant pressure drop.

Fig. 12 shows the comparison of spray distribution between three different flare angles. Significant differences can be found near the liner wall when changing θ. For θ of 8°, the spray presents a hollow cone structure with a large spray core angle. However, there are almost no fuel droplets dispersed at the region of R> 40 mm. This phenomenon may be related to the effects of high-speed jets that flow from the outer swirler and inner swirler on the dispersion of fuel droplets. It is known from the average flow field results that the opening angle of the outer swirl jets is low and the inner swirl stream gets weaker for θ=8°. Previous study has demonstrated that swirl plays an important role in fuel droplets transportation and atomization in a swirl cup [32]. It is deduced from flow-spray correlations that, in the case of θ=8°, fuel droplets do not have sufficient momentum from the inner swirl to move radially outward and will be transported downstream, restricting the fuel droplets from entering the outer swirl jets. For θ=25°, the spray also presents a hollow cone distribution, however, the cone angle is larger than that of θ = 8°, and fuel spray can impinge on the liner wall where the igniter locates. To conclude this section, authors suggest that the high-speed swirl jets can have a great impact on the spray distribution for separated dual-swirl flow. Smaller main stage flare angles induce smaller opening angles of outer swirl jets and weaker inner swirl jets, which blocks fuel droplets from transporting to the liner wall. Fuel droplets transportation in the separated dual-swirl is a complex phenomenon that is discussed in the following.

Fig. 13(a) and (b) shows the contour plots of spray distribution superimposed with axial velocity field for θ=8°, 25° at the pressure drop of 3% and FAR of 0.03. As shown, the fuel droplets are confined by the outer SWJ and cannot penetrate it to arrive at the corner. The highest

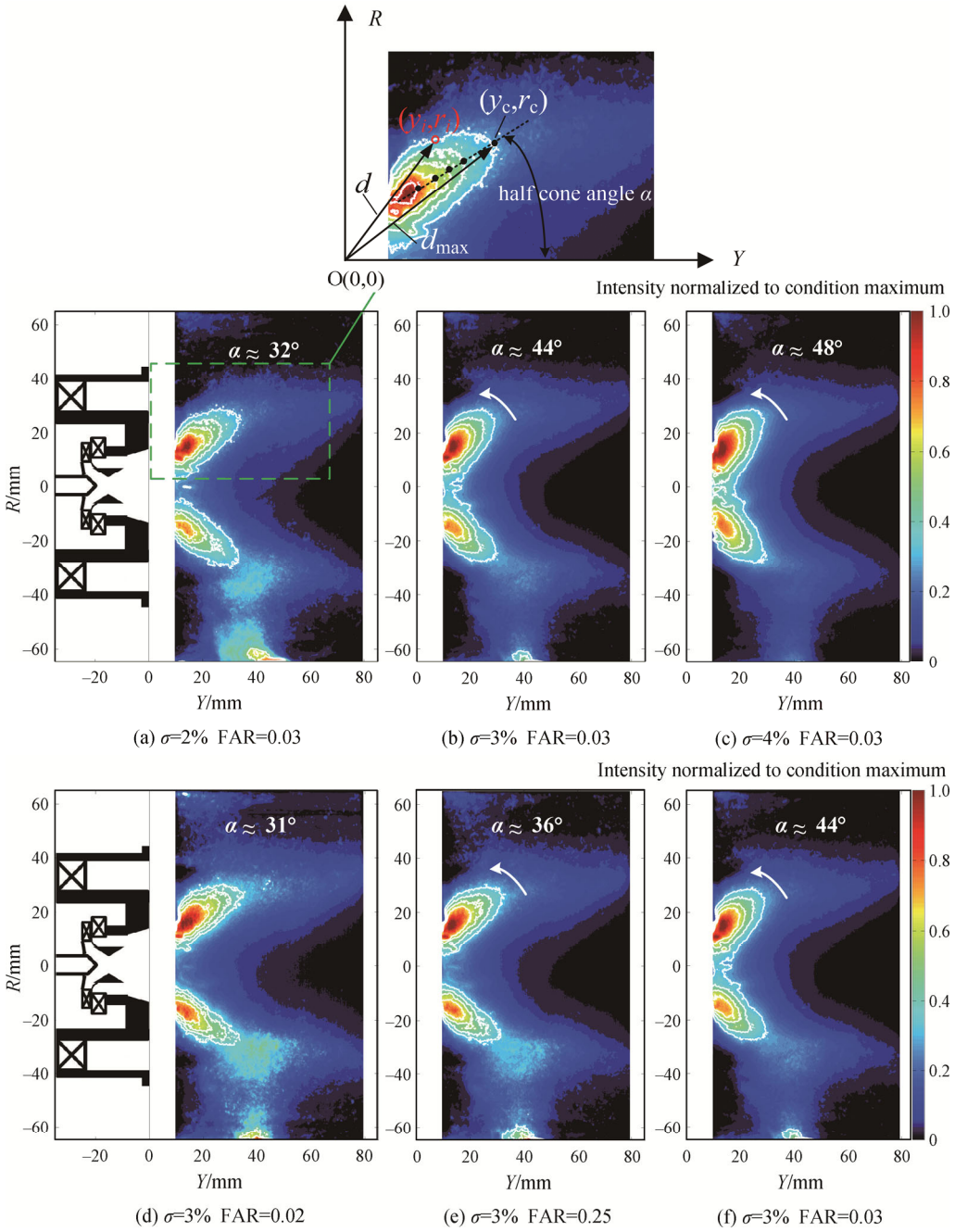

Fig. 10 PMie results with the main stage flare angle of 8°. (a)–(c) are the spray distribution with different pressure drops and (d)–(f) are the spray distribution with different FARs. All results are averaged by 500 images for each operating condition.

spray concentration is located in the IRZ. The backflow in IRZ restricts further downstream transportation of fuel droplets and forms the downstream boundary of spray cone. At the ISL inside the outer SWJ, there is a low-velocity path (red rectangle) suitable for droplet transportation. Transportation of fuel droplets along the ISL enables an appropriate droplet concentration at the wall (yellow square) in the case of θ=25°. The starvation of fuel droplets at the wall for θ= 8° demonstrates that the low radial velocity ratio in SWJ gives the droplets a lower radial momentum to move radially outward.

The stepwise atomization and droplets transportation of fuel spray in the centrally staged LPP combustor are analyzed. Only the pilot nozzle is fueled in the present study; the fuel atomization and transportation proceed as following. First the fuel is injected from the center simplex nozzle at a cone angle of 90° and the spray impinges on the venturi tube to generate a thin fuel film. Subsequent process is the film fragmentation through the aerodynamic shear between the counter-rotating swirls from the inner pilot stage. After the primary and secondary atomization, the big droplets are broken into

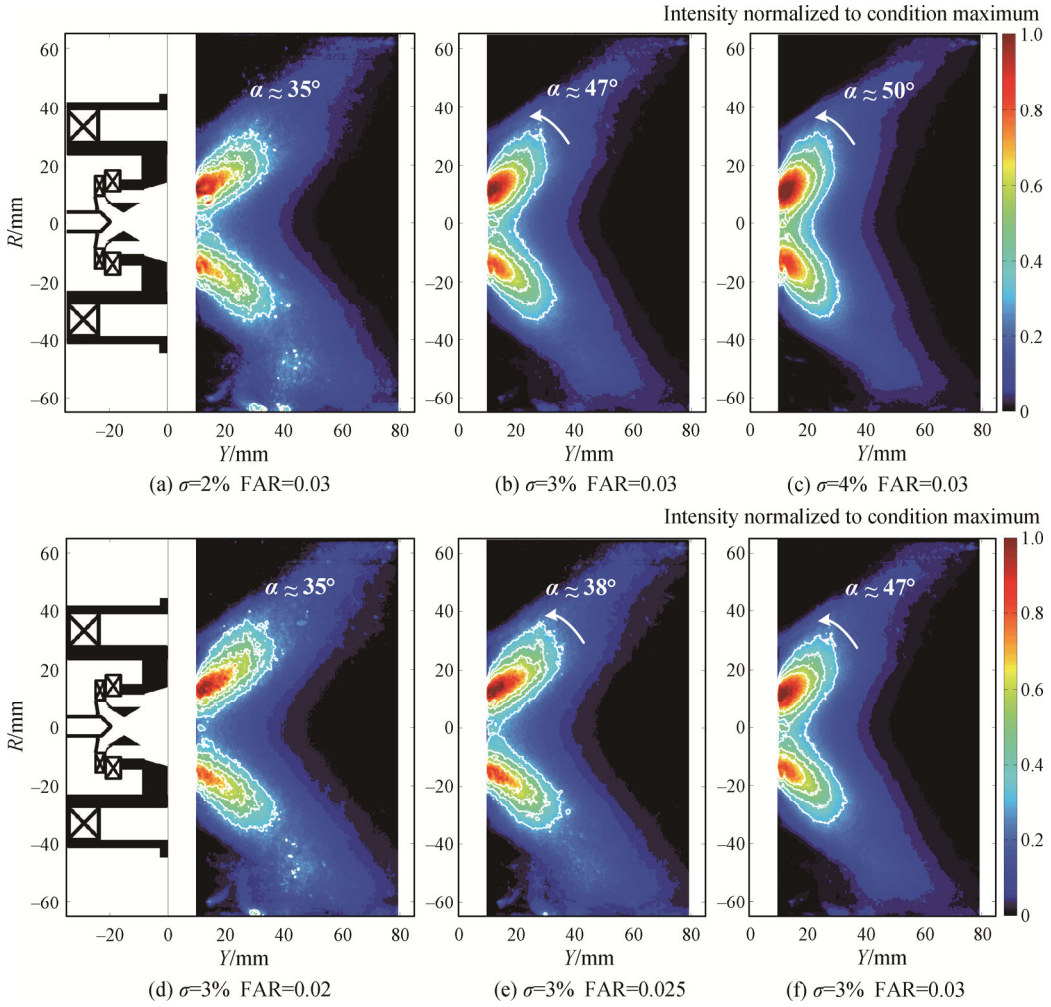

Fig. 11 PMie results with the main stage flare angle of 25°. Upper row is the spray distribution with different pressure drops and bottom row is the spray distribution with different FARs. All results are averaged by 500 images for each operating condition.

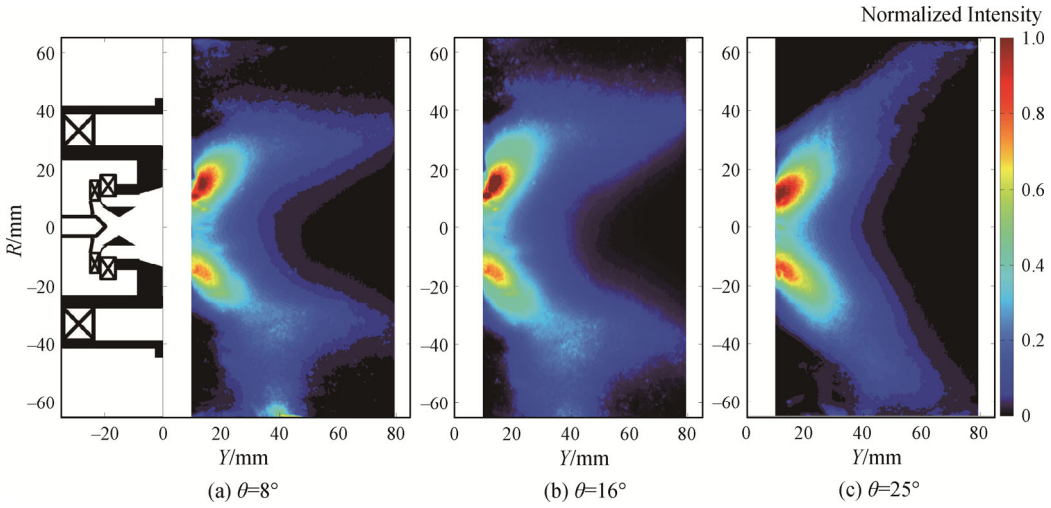

Fig. 12 PMie results with the outer stage flare angle of 8°, 16°, and 25° at the condition of σ=3% and FAR= 0.03. All results are averaged by 500 images for each case.

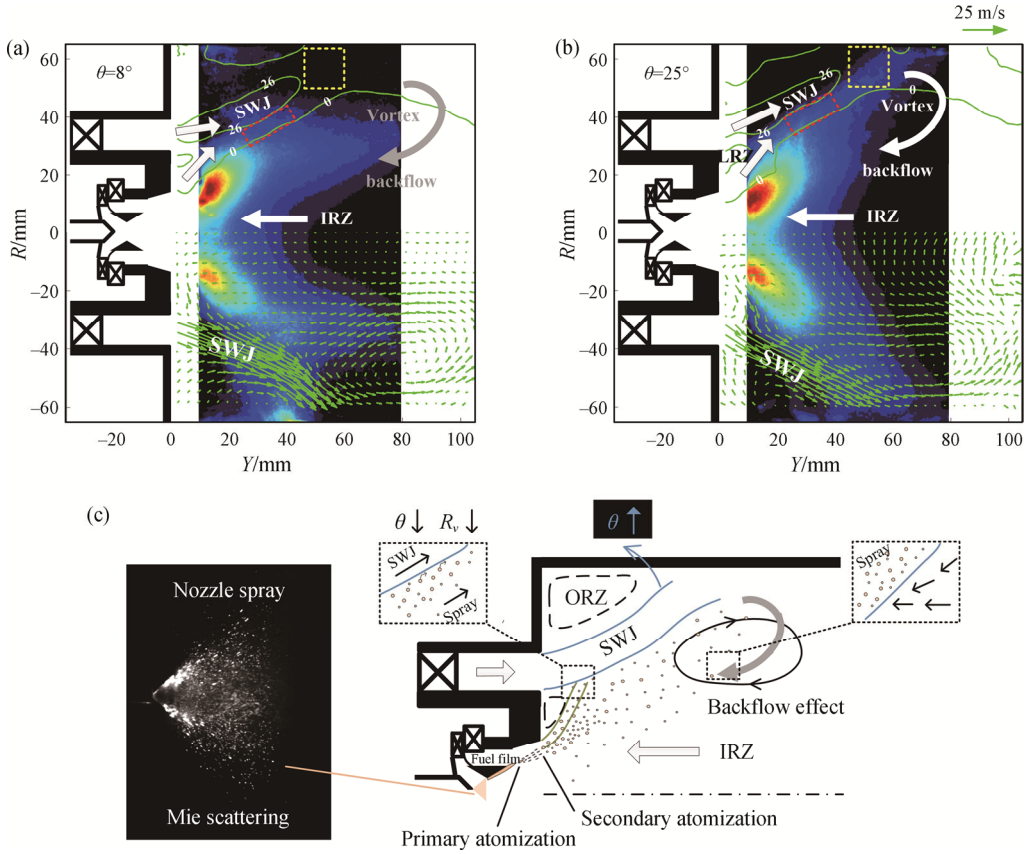

Fig. 13 Mean axial velocity superimposed with spray distribution (top) and velocity vectors superimposed with spray distribution (bottom) for (a) θ=8°, and (b) θ=25° at the condition of σ=3% and FAR=0.03. (c) Illustration of fuel atomization and transportation processes in the centrally staged LPP combustor

smaller droplets. The small droplets are then transported downstream under the entrainment of swirl flow. When the droplets reach the outer SWJ, the high-speed jet zone acts as an aerodynamic "wall" that droplets cannot penetrate. For the case of a large flare angle, the droplets can transport along the ISL and arrive at the wall. However, the decrease of flare angle reduces the radial velocity ratio R_v, which gives the droplets a higher axial momentum to transport downstream to the IRZ. Thus in the case of a small flare angle, the fuel droplets are not able to move along the ISL and arrive at the wall. Finally, as the droplets move to the vortex in IRZ, the downstream transportation is stopped by the reverse flow. From the above discussion, it is concluded that the outer SWJ and route along the ISL play important roles in transporting the fuel droplets to the igniter.

3.4 Flame morphology analysis

3.4.1 The whole ignition process

This section aims to have a full overview of ignition process in such complex swirl spray before identifying the effects of outer stage flare angle on the ignition process. Fig. 14 presents the flame area evolutions of two successful ignition processes for θ=25° and 8°. The ignition unit applied in the present study gives sparks with the duration of about 119 μs, thus the high-speed camera is not able to capture the kernel formation process with a frequency of 6 kHz. The plots begin at the moment that a kernel is successfully generated. A successful kernel formation is defined as a self-sustained kernel being formed after a spark has stopped delivering energy. Some important moments need to be defined in the present study for a detailed description of the ignition process. The moment t_1 is defined as the moment of a spark triggered by the igniter; 0 ms is defined as the moment of a kernel is successfully generated; t_2 and t_3 are defined as the first and last moments that the flame area is below the critical value (9100 pixels), and t_4 is defined as the moment that the flame area firstly exceeds 10^5 pixels.

It is seen from Fig. 14 that a successful ignition event in the combustor contains five necessary phases: the kernel formation P1, the early kernel propagation P2, the growth delay P3, the flame growth P4, and the flame stabilization P5. At the first phase of ignition, the breakdown provides a plasma zone of high temperature,

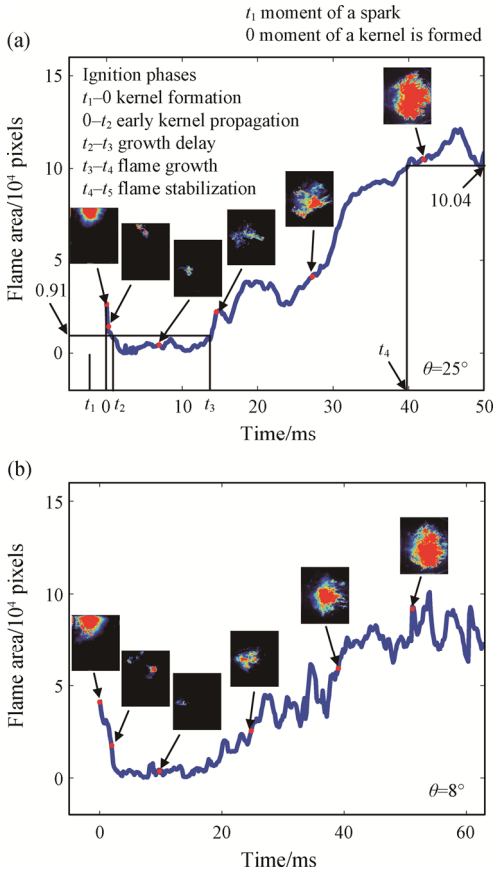

Fig. 14 Evolution of flame area of two successful ignition processes for (a) θ=25° and (b) θ=8°. The division of the whole ignition process is given.

which ignites the flammable fuel-air mixture to generate a flame kernel. Once a kernel is successfully generated, phase P2 begins and the flame area begins to decrease sharply to a low value. During this period, the flame kernel is observed to leave the liner wall and propagate towards the downstream. After a certain time of kernel propagation, the special "growth delay" phase P3 begins, during which the kernel remains low light emission without growth. After the "growth delay" phase, the flame area begins to increase continuously in the flame growth phase P4. Finally, it comes to the flame stabilization phase P5, which is the end of the successful ignition process.

Comparing the overall ignition process between the two flare angles, the time that the flame growth begins for θ=8° is later than that for θ=25°. Moreover, the flame kernel seems a different behavior at the early phase of propagation for two configurations. With the ignition phases being defined, the present study aims to identify the effects of flare angle on the kernel propagation and growth delay, which is discussed in the following.

3.4.2 Flame kernels propagation

The flare angle is varied from θ=8° to 25° and flame propagation is revealed by the high-speed images. Fig. 15 shows two kernel propagation processes for different flare angles of the outer stage: θ=8° and θ=25° respectively. The image sequence starts at 0 ms after a kernel is successfully generated and different time intervals are chosen to better illustrate the flame propagation mechanism. The spark is triggered at the liner wall (Y= 50 mm, R=65 mm). The typical kernel propagation process is revealed from the images. The first image shows a bright kernel produced by the spark, then the flame kernel begins to leave the liner wall and propagate downstream due to the main swirl jets. After a certain time, the flame kernel starts to propagate upstream towards the nozzle with the flame emission intensity decreasing continuously. Once the kernel moves to the nozzle, a special delay phase begins during which a weak kernel remains in the center without growing. The general features of the kernel propagation process are similar to those observed in laboratory-scale methane flames [8, 15], and in model gas turbine combustors [5, 6].

Comparing the kernel propagation between the two configurations, it is found that the flame kernel spends a longer time (2.7 ms) propagating downstream before it travels upstream for the small flare angle (θ=8°). For both gaseous and spray ignition, successful ignitions are associated with a flame kernel being captured by the recirculating flow. The longer time propagating downstream at the early period of ignition means that the kernel needs a longer time reaching the recirculation zone, which may lead to a higher risk of ignition failure.

The flame kernel trajectories and velocities provide important information that explains the process of subsequent flame propagation after the kernel is formed. The kernel trajectory and velocity are processed from a sequence of high-speed flame images, as sketched in Fig. 16(a) (detailed in Section 2.4). The colors of the arrows in Fig. 16(b) and Fig. 16(c) indicate the time and the velocity magnitude respectively. Two different flame kernel propagation routes have been identified from kernel trajectories in Fig. 16(b): the shorter route for large flare angle (θ=25°), and the longer route for small flare angle (θ=8°). The flame kernel is blown to a longer distance downstream (Y≈90 mm) before propagating upstream when the flare angle is 8°. From Fig. 16(c), it is seen that the kernel velocity accelerates at the early phase of propagation and decelerate when the kernel moves to the center of combustor. A higher kernel velocity up to 38.9 m/s is observed (green oval) during the downstream propagation for θ=8°. The downstream movement trend of ignition kernels for θ=8° is also seen in the propagation regions in Fig. 16(d).

These two different flame kernel trajectories and velocities result from different flow fields and spray distributions. It has been demonstrated that flame kernel motion is dominated by convection rather than propagation [6], which emphasizes the importance of

cold flow to flame kernel propagation. Smaller angles of outer swirl jets are formed with the IRZ being shifted downstream for θ=8°, as shown in Fig. 5. Hence, from the perspective of aerodynamics, once a kernel is generated by a spark in the case of θ=8°, it will be transported by the outer swirl jets to a longer distance downstream before it propagates upstream following the recirculating flow. Regions with appropriate mixture fraction and small droplet size are favorable for spray ignition [15]. The U shape spray distribution might be another factor causing the kernel to propagate downstream a longer distance to find the appropriate fuel-air mixture when θ is 8°. Longer flame propagation route will increase the heat dissipation and the risk of blown out before the kernel is captured by the recirculating flow. The increased flame propagation distance for θ=8° partly explains the worse ignition performance in this case.

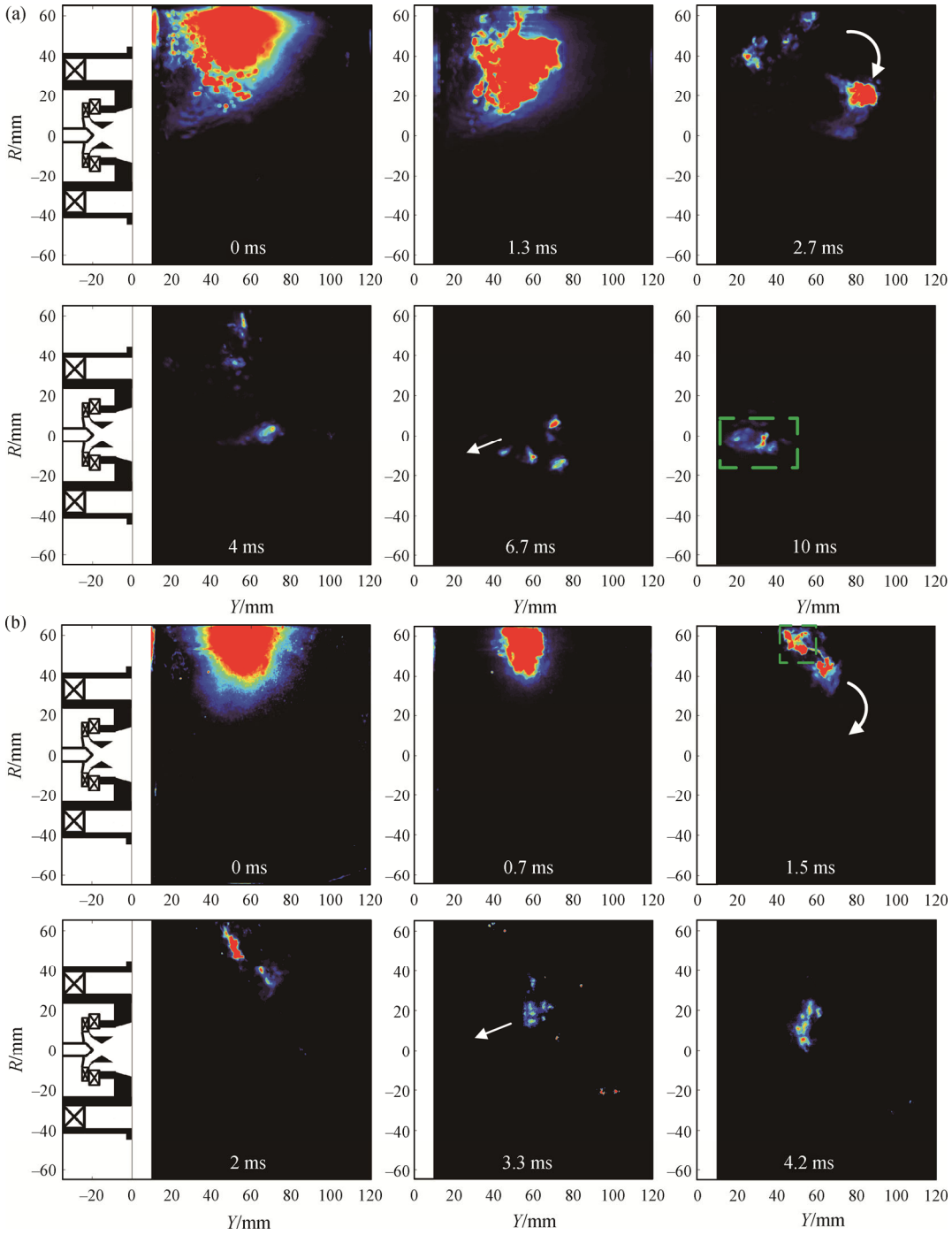

Fig. 15 High-speed spontaneous flame emission images: the flame propagation comparison between (a) θ=8° and (b) θ=25°

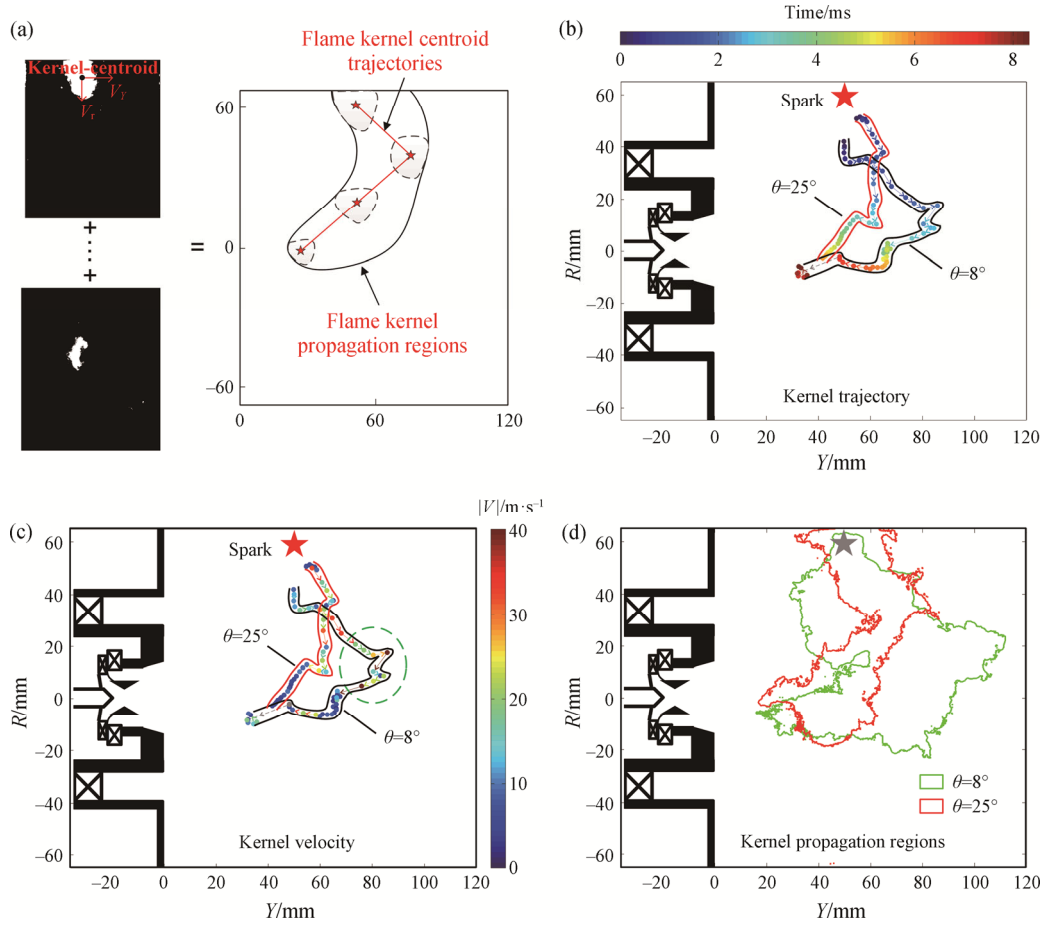

Fig. 16 Kernel-tracking process (a). Evolution of ignition kernel during the propagation process for θ=8° and θ=25°: (b) centroid trajectories, (c) velocity vectors, and (d) propagation regions

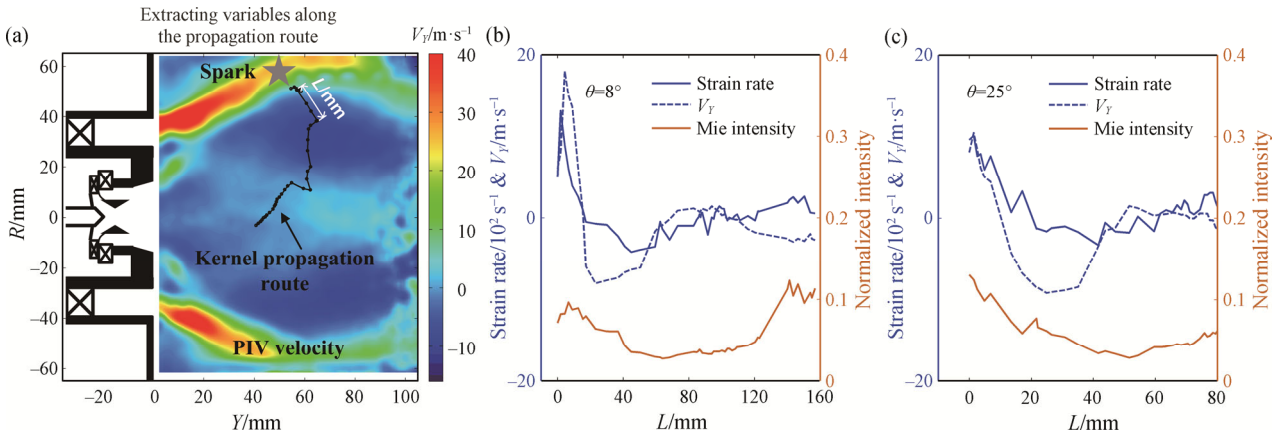

Fig. 17 Example of extracting axial flow velocity along the kernel propagation route (a). Time-averaged variables of axial velocity, strain rate, and Mie scattering intensity from spray extracted along the flame kernel propagation route for (b) θ=8° and (c) θ=25°

To further reveal the correlation between flame kernel propagation and the flow and spray, the time-averaged axial velocity, strain rate, and Mie scattering intensity from spray are extracted at each centroid position along the flame kernel propagation route, as shown in Fig. 17(a). The extracted velocity and spray variables are plotted as a function of kernel propagation distances L (Fig. 17(b) and (c)). It is seen that the kernel propagates from a high-velocity jet zone to the low-velocity central recirculation zone. High strain rates and velocities are not

supportable for kernel survival. In the case of θ=8°, the strain rate at the beginning of the kernel propagation is higher up to 1312 s^{-1} and the axial velocity can reach 18 m/s, leading to a worse ignition performance. This confirms that although swirl can create a recirculation zone for flame stabilization, the swirl jet is a barrier for ignition and flame propagation for the high strain rate and velocity.

It should be noted that the special phase of weak flame kernel anchoring in the combustor center is an interesting phenomenon. This behavior has been observed in previous spray flames [6, 7, 9]. Further analysis on this "growth delay" phase is presented. Fig. 18 shows the high-speed flame images during the growth delay phase for two configurations (θ=8° and θ=25°). The flame kernel is observed moving in the center of the combustor

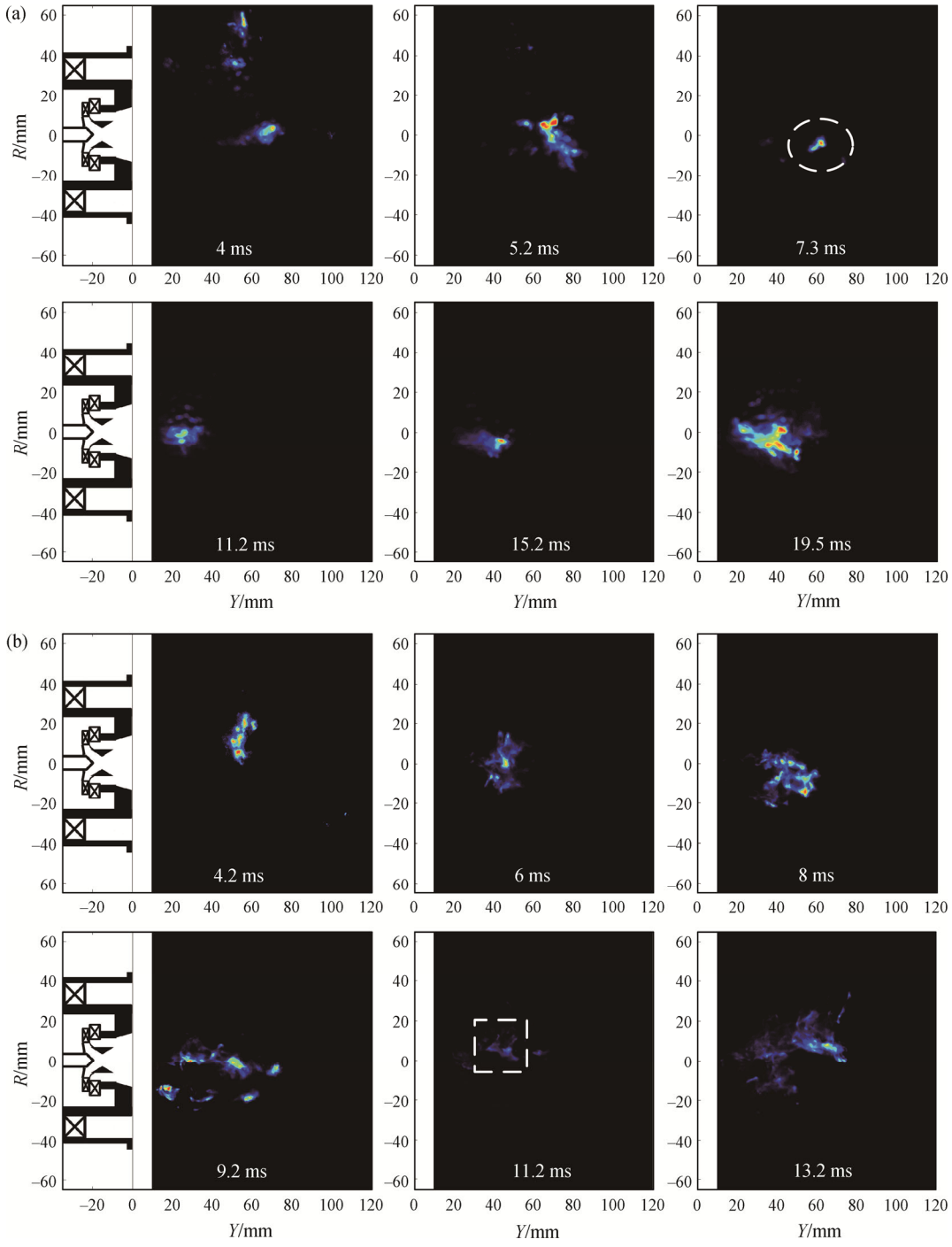

Fig. 18 High-speed spontaneous flame emission images of the growth delay phase for (a) θ=8° and (b) θ=25°

and emitting very little light. From the location and shape of the flame kernel, the "growth delay" phase might be understood as the flame root stabilization process. Looking from the whole ignition process, the flame kernel is the lowest in size and light intensity during the "growth delay" phase (see Fig. 14), which highlights the importance of the period of flame root stabilization. This agrees with the results of Stöhr et al. [33], who found that flame root plays a crucial role in the stabilization of swirl flame and extinction of flame root will lead to flame blowout. No obvious differences in flame morphology during the "growth delay" phase are found between the two flare angles. Nevertheless, the duration of the "growth delay" phase for θ=8° is approximately 15.5 ms, which is longer than that for θ=25° (≈9 ms). Detailed discussion of the underlying mechanism leading to "growth delay" is needed in the future, which is beyond the scope of the present study.

3.5 Discussion

The effects of outer stage flare angle on the ignition and flame propagation in the separated dual-swirl spray will now be discussed from the perspective of aerodynamics and spray dispersion. Two sketches are proposed to illustrate the main conclusions extracted from results above, as shown in Fig. 19. Previous studies of forced ignition in gaseous flames [8, 29] and liquid flames [15] have demonstrated that regions of high velocity are unfavorable for flame kernel to survive and propagate upstream. For the centrally staged combustor investigated in this work, it is concluded that the outer swirl jets from the outer stage are characterized by high strain rates and velocity magnitude, which have a significant influence on spray distribution and flame propagation. First, there is not enough momentum for fuel droplets to penetrate through jets, so the spray is confined by outer swirl jets. Second, a flame kernel in jets flow will first move downstream and then propagate upstream, which is identified in the literature [34]. For small flare angle, the outer swirl jets shift inward, transporting the kernel a longer distance downstream before it is captured by the recirculating flow (see Fig. 16), leading to a longer propagation route. A larger outer stage flare angle induces larger opening angles of outer swirl jets. Consequently, a fuel-rich zone is formed near the igniter, which is beneficial for kernel generation. ORZ has been proved to be an unfavorable region for achieving ignition in bluff-body flames [29]. A larger size of IRZ and a smaller size of ORZ are formed for a large flare angle, creating a better flow condition for kernel generation and flame propagation. Based on the different non-reacting flow and spray distribution, the flame propagation exhibits a short-route propagation for the large flare angle while the long-route propagation is observed for the small flare angle. Aerodynamically, it is concluded that the lower outer swirl radial velocity ratio is not favorable for the upstream propagation of flame kernel, thereby deteriorating the ignition performance.

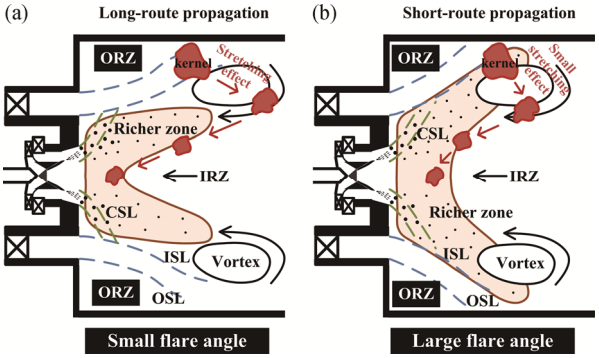

Fig. 19 Sketch of the behavior of flame propagation for different flare angles: the long-route propagation (a) and the short-route propagation (b)

The results in the present study show that the outer swirl jets have a great influence on the lean ignition limit and the ignition process in a separated dual-swirl spray flame, which results from changes in aerodynamics and spray distribution. These findings may be extended to universally used swirl-stabilized combustors. Forced ignition in gas turbine combustors are usually realized by surface-discharge igniters that produce multiple sparks at the liner wall. Fig. 20 summarises the results focusing on the roles of swirl jets in the spark ignition of swirl flame. Although swirl is important for flame stabilization, the high strain rate and starvation of fuel in swirl jets can lead to worse ignitability (spark location at dashed red circle). The effective strategy for solving this issue is shifting the swirl jet zone upstream. The present study suggests that the increase of the swirl radial velocity ratio can facilitate spark ignition in a swirl-stabilized combustor. For combustor designers, this can be accomplished by increasing the flare angle of the swirler annular channel.

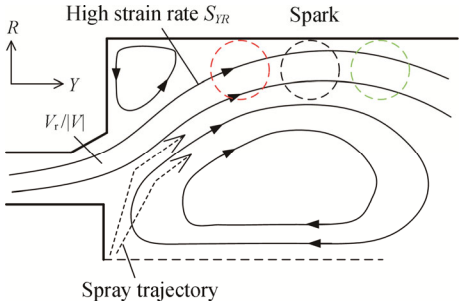

Fig. 20 Sketch summarising the roles of swirl jets in the spark ignition in swirl-stabilized combustors superimposed on a schematic of velocity pattern and the spray dispersion. Ignition is initiated by sparks located along the liner wall.

4. Conclusions

The effects of outer stage flare angle on the ignition and flame propagation in a separated dual-swirl spray flame have been experimentally investigated. Three flare angles of θ=8°, 16°, 25° are studied in the present work. The ignition performance improves when the flare angle is larger. Flame area evolutions show that a successful ignition event contains five necessary phases: kernel formation, early kernel propagation, growth delay, flame growth, and flame stabilization. The kernel centroid trajectories and propagation regions demonstrate that the kernel travels a longer distance downstream before it propagates towards the nozzle for a smaller flare angle. A longer time is identified during the growth delay phase for a lower θ.

The velocity field is characterized by a typical confined dual-swirl containing three main recirculation regions and two swirling jets. The spray distribution features a hollow cone pattern with the outer edge blocked by the swirl jets. The smaller flare angles (θ=8°) induce smaller opening angles of swirl jets that isolate fuel droplets from the liner wall, yielding a fuel-lean zone near the igniter. Correlation of the flame kernel propagation route and the flow properties illustrates that the strain rates and velocity are high at the early phase of propagation and decrease to a low value as the kernel propagates to the center. Although swirl can create a recirculation zone for flame stabilization, the outer swirl jet from the outer stage is characterized by high strain rates up to 1312 s^{-1} and low spray concentrations, and thus is not favorable for flame kernel survival and propagation during the kernel propagation phase. Increasing the swirl radial velocity ratio to change swirl jets patterns is an effective way for optimizing ignition performances in swirl-stabilized combustors and this can be accomplished by the design of a larger flare angle. The results in the present work can help understand the roles of swirl jets in the spark ignition in a dual-swirl spray flame and provide guidance in improving ignition performances in swirl-stabilized combustors.

Acknowledgements

This work was supported by National Natural Science Foundation of China (Grant No. 91641109) and National Science and Technology Major Project (2017-III-0004-0028).

References

[1] Liu Y., Sun X., Sethi V., et al., Review of modern low emissions combustion technologies for aero gas turbine engines. Progress in Aerospace Sciences, 2017, 94(10): 12–45.

[2] Mastorakos E., Forced ignition of turbulent spray flames. Proceedings of the Combustion Institute, 2017, 36(2): 2367–2383.

[3] Lefebvre A.H., Gas turbine combustion, 2nd ed. Taylor and Francis, London, 1999.

[4] Mastorakos E., Ignition of turbulent non-premixed flames. Progress in Energy and Combustion Science, 2009, 35(1): 57–97.

[5] Wang B., Zhang C., Lin Y., et al., Influence of main swirler vane angle on the ignition performance of TeLESS-II combustor. Journal of Engineering for Gas Turbines and Power, 2017, 139(1): 011501.

[6] Read R.W., Rogerson J.W., Hochgreb S., Flame imaging of gas-turbine relight. AIAA Journal, 2010, 48(9): 1916–1927.

[7] Mosbach T., Sadanandan R., Meier W., et al., Experimental analysis of altitude relight under realistic conditions using laser and high-speed video techniques. Proceedings of the ASME Turbo Expo 2010: Power for Land, Sea, and Air, Glasgow, UK, 2010, Paper No: GT2010-22625.

[8] Ahmed S.F., Balachandran R., Marchione T., et al., Spark ignition of turbulent nonpremixed bluff-body flames. Combustion and Flame, 2007, 151(1–2): 366–385.

[9] Naegeli D.W., Dodge L.G., Ignition study in a gas turbine combustor. Combustion Science and Technology, 1991, 80(4–6): 165–184.

[10] Wang X., Lin Y., Zhang C., et al., Effect of swirl cup's secondary swirler on flow field and ignition performance. Journal of Thermal Science, 2015, 24(5): 488–495.

[11] Liu C., Liu F., Yang J., et al., Experimental investigation of spray and combustion performances of a fuel-staged low emission combustor: effects of main swirl angle. Journal of Engineering for Gas Turbines and Power, 2017, 139(12): 121502.

[12] Fu Z., Lin Y., Li J., et al., Experimental investigation on ignition performance of LESS combustor. Proceedings of the ASME Turbo Expo 2011: Turbine Technical Conference and Exposition, Vancouver, Canada, 2011, Paper No: 2011-45786.

[13] Chterev I., Foley C., Foti D., et al., Flame and flow topologies in an annular swirling flow. Combustion Science and Technology, 2014, 186(8): 1041–1074.

[14] Fan X., Xu G., Liu C., et al., Experimental investigations of the flow field structure and interactions between sectors of a double-swirl low-emission combustor. Journal of Thermal Science, 2020, 29(1): 43–51.

[15] Marchione T., Ahmed S., Mastorakos E., Ignition of turbulent swirling n-heptane spray flames using single and multiple sparks. Combustion and Flame, 2009, 156(1): 166–180.

[16] Collin-Bastiani F., Marrero-Santiago J., Riber E., et al., A

joint experimental and numerical study of ignition in a spray burner. Proceedings of the Combustion Institute, 2019, 37(4): 5047–5055.

[17] de Oliveira P.M., Mastorakos E., Mechanisms of flame propagation in jet fuel sprays as revealed by OH/fuel planar laser-induced fluorescence and OH chemiluminescence. Combustion and Flame, 2019, 206(8): 308–321.

[18] Liu C., Liu F., Yang J., et al., Investigations of the effects of spray characteristics on the flame pattern and combustion stability of a swirl-cup combustor. Fuel, 2015, 139: 529–536.

[19] Mongia H., TAPS-A 4th generation propulsion combustor technology for low emissions. AIAA International Air and Space Symposium and Exposition: The Next 100 Years, Dayton, Ohio, USA, 2003, Paper No. 2003-2657.

[20] Lazik W., Doerr T., Bake S., Low NO_x combustor development for the engine 3E core engine demonstrator. XVIII International Symposium on Air Breathing Engines (ISABE), Beijing, China, 2007, pp. 2–7.

[21] Mi X., Zhang C., Wang B., et al., Influence of main stage air splits on the ignition performance of TeLESS-II combustor. Proceedings of the ASME Turbo Expo 2017: Turbomachinery Technical Conference and Exposition, Charlotte, North Carolina, USA, 2017, Paper No. GT2017-63216.

[22] Zhang C., Mi X., Hui X., et al., Characterizing particulate matter emissions in an aviation kerosene-fueled model combustor at elevated pressures and temperatures. Fuel, 2019, 241: 227–233.

[23] Yang S., Zhang C., Lin Y., et al., Experimental investigation of the ignition process in a separated dual-swirl spray flame. Combustion and Flame, 2020, 219: 161–177.

[24] Otsu N., A threshold selection method from gray-level histograms. IEEE Transactions on Systems Man and Cybernetics, 2007, 9(1): 62–66.

[25] Baum M., Poinsot T., Effects of mean flow on premixed flame ignition. Combustion Science and Technology, 1995, 106(1–3): 19–39.

[26] Billant P., Chomaz J.M., Huerre P., Experimental study of vortex breakdown in swirling jets. Journal of Fluid Mechanics, 1998, 376: 183–219.

[27] Huang Y., Yang V., Dynamics and stability of lean-premixed swirl-stabilized combustion. Progress in Energy and Combustion Science, 2009, 35(4): 293–364.

[28] Tangirala V., Chen R.H., Driscoll J.F., Effect of heat release and swirl on the recirculation within swirl-stabilized flames. Combustion Science and Technology, 1987, 51(1–3): 75–95.

[29] Ahmed S.F., The probabilistic nature of ignition of turbulent highly-strained lean premixed methane-air flames for low-emission engines. Fuel, 2014, 134: 97–106.

[30] Stojkovic B.D., Sick V., Evolution and impingement of an automotive fuel spray investigated with simultaneous Mie/LIF techniques. Applied Physics B, 2001, 73: 75–83.

[31] Jermy M.C., Greenhalgh D.A., Planar dropsizing by elastic and fluorescence scattering in sprays too dense for phase doppler measurement. Applied Physics B, 2000, 71: 703–710.

[32] Becker J., Hassa C., Experimental investigation of spatial and temporal aspects of the liquid fuel placement in a swirl cup at elevated pressure. Proceedings of the ASME Turbo Expo 2004: Power for Land, Sea, and Air, Vienna, Austria, 2004, Paper No. GT2004-53524.

[33] Stöhr M., Boxx I., Carter C., et al., Dynamics of lean blowout of a swirl-stabilized flame in a gas turbine model combustor. Proceedings of the Combustion Institute, 2011, 33(2): 2953–2960.

[34] Ahmed S.F., Mastorakos E., Spark ignition of lifted turbulent jet flames. Combustion and Flame, 2006, 146(1–2): 215–231.